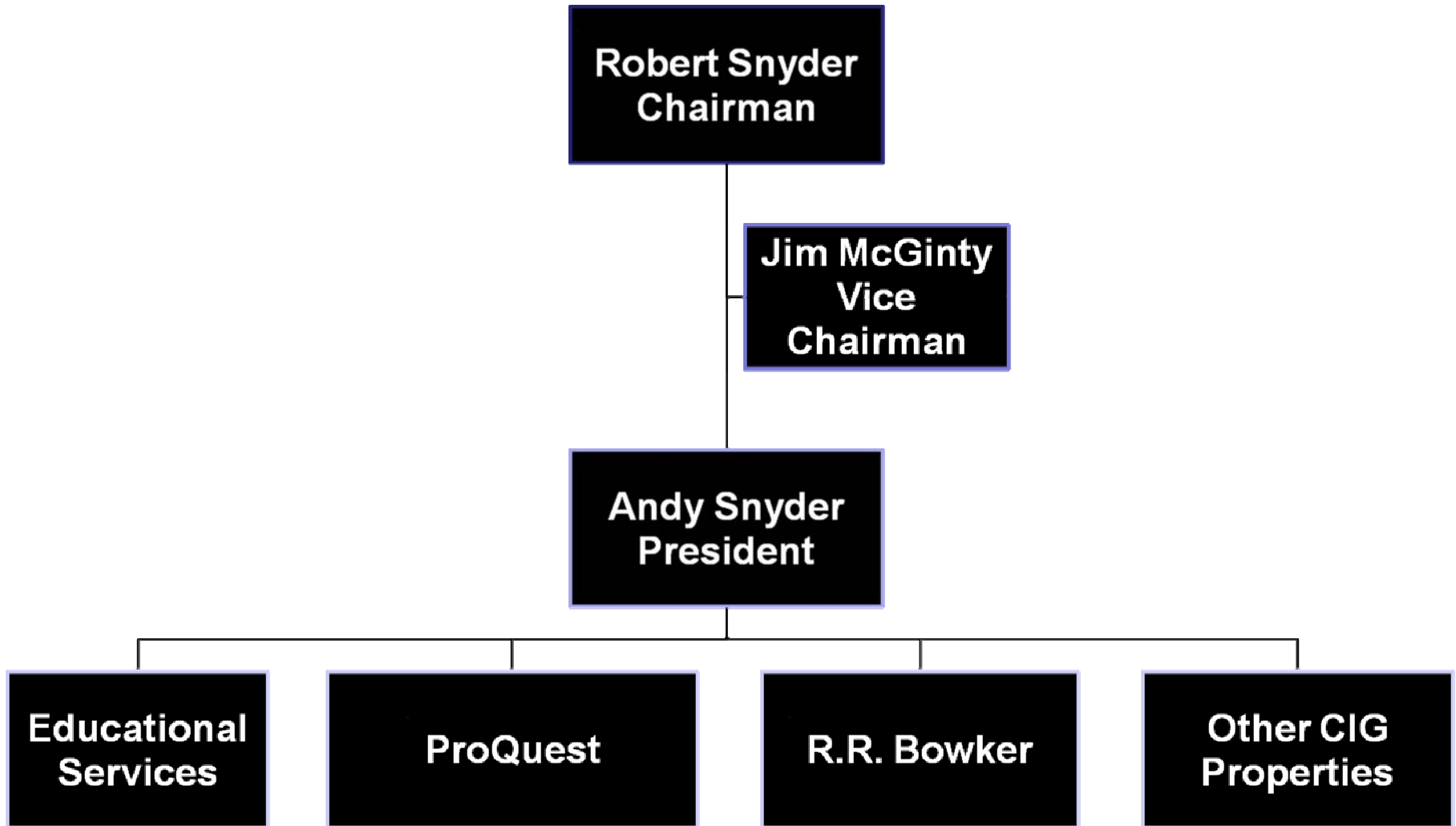


Presentation Will Cover...

- Description of Deep Indexing
- Discuss its use in the marketplace
- Initial reaction from users/customers
- Impact on Secondary Publishing



Extracting/Structuring data presented in tables and figures within published literature

45 T. Ueda, K. Nozaki, H. Matsuda: Characteristics at finite temperature in quenched lattice QCD

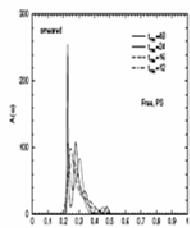


Fig. 2. The result of MEM analysis for the spectral function from the smeared PS correlation composed of five quarks at $T = 0$.

quarks, the width extracted with MEM may be of order of 0.05-0.1 in temporal lattice units. We also apply the χ^2 fit analysis to the correlation composed of five quarks. In this case the errors of the same size as in Monte Carlo simulation are just put on the correlators without fluctuating them. Figure 3 shows the result of the χ^2 fit of the correlation composed of five quarks at $N_t = 26$ using the 1- βW smearing. The χ^2_{min} dependence of mass and width (with fixed $\tau_{fit} = 1$) indicates that the single βW smearing does not fit the correlators. As is observed in Fig. 3, if the correlator is composed of five quarks, the χ^2 fit gives smaller difference in mass and width parameters for the smeared as well as non-smeared correlators. This dependence is in agreement with the fact that the propagator should only show the two free quark cut and no particle-like resonances and indicates that by testing the dependence of the result on the smearing function we can distinguish physical effects from artifacts due to smearing.

5 Setup of numerical simulation

5.1 Lattice setup

The zero temperature lattice used in this paper is the third one of [14], a quenched lattice of size $20^3 \times 16$, prepared with the standard plaquette action with $(\beta, g_0) = (6.10, 2.208)$. These coupling and bare mass are correspond to the renormalized anisotropy $\xi = a_0/a_4 = 4$ within 1% accuracy [57], and the spatial lattice cutoff $a^2 = 2.008(19)$ GeV² set by the hadronic radius r_0 [58]. At $T = 0$, 500 configurations are generated with the pseudo-Hermitian update algorithm, with separated by 2000 sweeps after 2000 sweeps for thermalization. The mean-field values are defined as the average value of link variables in the London phase, and obtained at $\tau_0 = 0.800(1)$ and $\tau_0 = 0.99(2)$.

To determine the critical temperature, we measure the Polyakov loop susceptibility at $N_t = 27, 28$, and 29 at $\beta = 6.10$ and add them, at several values of β (with corresponding values of g_0) around $\beta = 6.10$ at $N_t = 28$. At $\beta = 6.06$ the lattice scale set by r_0 is $a^2 = 1.860(19)$ GeV², which together with $\tau_0 = 1$ at $\beta = 6.10$ determine the scales at the other values of β by linear interpolation. The susceptibility peaks at about $\beta = 6.10$ and $N_t = 28$. The critical temperature is obtained as $T_c = 290$ MeV with 10 MeV of roughly estimated uncertainty. This value is slightly higher than the conventional values by the scale set by the string tension, as a common tendency by adjusting the scale by r_0 .

The characteristic temperatures at $T_c > 0$ are measured for two values of temporal lattice extent, $N_t = 22$ and 26. Corresponding temperatures are 1.8(2), for $N_t = 22$, and 1.0(2), for $N_t = 26$. For brevity, these temperatures are hereafter referred to as T_c^{22} and T_c^{26} , respectively. These temperatures treated in this paper are in the vicinity of the transition. At each of these N_t 's, we generate 2000 configurations each separated by 500 pseudo-bulk-sweep after 2000 sweeps for thermalization.

S. Bratsman et al.: The 1996-1999 ENSO cycle in a classical climate model

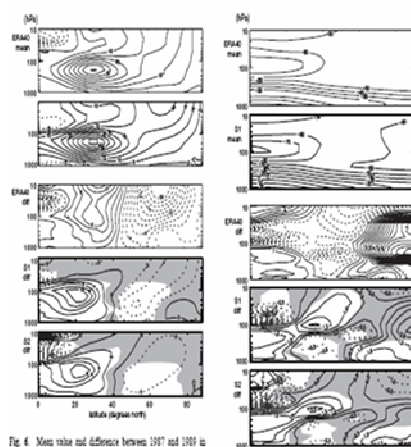


Fig. 6. Mean value and difference between 1997 and 1999 in total mean sea level (m), averaged from January to March in ERA40. S1 and S2. Shaded areas are not significantly different from zero ($p < 0.05$).

ties than for the westerly phase). Study-one SOCCOL simulations without GSO (and hence temperature anomalies) found a stronger northern anticyclonic pole vortex for solar maximum conditions compared to solar minimum conditions (Eppers et al., 2004), but the signal is not statistically significant and clearly smaller (around 1 m) than that in our simulation. Hence, solar irradiance changes do not seem to be sufficient to explain the signal.

Small mean temperature differences between El Niño and La Niña are shown in Fig. 7. The observations show a pronounced signal in the Arctic lower stratosphere. In S1, the pattern is well reproduced, but not in strength, whereas in S2 the pattern is less well reproduced. The Arctic temperature response in the model is significant below 200 hPa. At larger levels, within-resolvable variability is too large to obtain significant results. Both S1 and S2 show a significant warming of the stratospheric response and lower stratosphere which is not observed in the observations. This is probably related to the overestimated displacement of the subtropical jet in the model (Fig. 6) that is not seen in the observations.

477

S. Bratsman et al.: The 1996-1999 ENSO cycle in a classical climate model

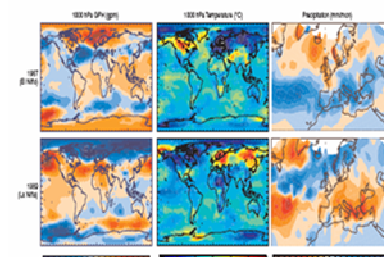


Fig. 7. Observed anomalies of 1000-hPa geopotential height (left) and sea surface temperature (middle), as well as precipitation (right) for January to March 1997 (top) and January to March 1999 (bottom), with respect to the 1979-2002 period.

March 1997 and 1999. The two winters exhibit the well known ENSO signal in the North Pacific area such as a strong (weak) Aleutian low for El Niño (La Niña), accompanied by high (low) temperatures in Alaska. Temperature anomalies in midwestern Europe were strongly negative for the El Niño winter and positive for the La Niña winter. The 1000-hPa GPH field shows a pronounced negative (positive) NAO pattern in the two winters. This is in excellent agreement with the "canonical" effect of ENSO on Europe in late winter. The El Niño winter also resembles the strong 1940-1942 case (Stouffer et al., 2004). A strong precipitation signal is found especially for the La Niña winter, with negative anomalies throughout the North Atlantic and mid-positive anomalies in southwestern Europe. The El Niño year shows anomalies of opposite sign, but slightly weaker in magnitude. In general, the results show a close symmetric response for these two winters with respect to each of the hemispheres, and they again support that 1996-1999 was a "classic" ENSO cycle with respect to its effect on the circulation over the North Atlantic-European sector.

In order to understand the modified Arctic temperature response in the stratosphere, we analyzed 12-monthly mean of temperatures at the North Pole ($87^{\circ}E$, $87^{\circ}W$) in SOCCOL at 10 hPa and 100 hPa in the individual ensemble members as well as in ERA40 (Fig. 8). The results show that 1998-97 show a strong disturbance (major anomalous warming) in January. While at 10 hPa, temperatures dropped again during February and reached very low values in March, the disturbance at 100 hPa persisted into spring. In 1999-99, in contrast, the polar stratosphere was undisturbed and cold well into February, but the final warming there was very pronounced. In the SOCCOL experiment major warmings appear in most of the simulations in both winters, consistently in late January/December. The large day-to-day variability causes a large winter-to-winter variability, which hampers the statistical analysis of ensemble means.

Comparisons between simulations and observations for the two individual winters are not possible in a strict sense (and therefore our claims below) because of the different climatologies used. Nevertheless, it is interesting to see that similar to the observations, both models show a response that is close to symmetric around the respective climatology in the two winters. Model results (ensemble means) are compared to the observations in Fig. 9 in the form of the difference between the El Niño winter (1997) and the La Niña winter (1999). The amplitude of the anomalies is generally smaller in the ensemble means than in the observations,

Atmos. Chem. Phys., 6, 4669-4685, 2006

www.atmos-chem-phys.net/6/4669/2006/

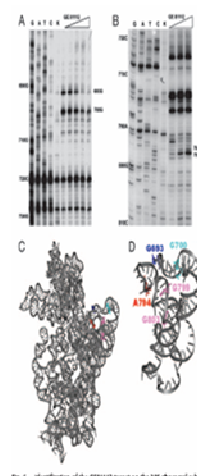


Fig. 8. Identification of the GPH signal on the 200 observed winters. The 1000-hPa base value (anomaly with respect to the 1979-2002 period) is affected by GPH-10, which is defined by linear regression analysis. (A) The location of the 200 winters (the 20 winters of the entire 2000 data set) and of the observation axis of the figure (S1 and S2) are also indicated (cf. Aramaki et al., 2005).

which is expected due to smearing. The pattern, however, are relatively well reproduced by both models. For El Niño winters in Niña, all experiments show cold winters in northeastern Europe, extending all across northern Britain, and a dipole pattern in 1000-hPa GPH resembling the pattern made of the NAO (see Compeau et al., 2001, for a discussion of related changes in subsurface variability). In the SOCCOL experiment, the signal is the observation (but at S1), the mainly changes the close to Iceland and the Azores. For precipitation (Fig. 7), all experiments reproduce the observed decrease in heavy and the increase in the Mediterranean area. The precipitation signal over the Atlantic ocean is a southeast shift in the Atlantic mean rain for El Niño relative to La Niña, which was also shown by Compeau and Srinivasan (2004). As for the other fields, the magnitude of the precipitation anomalies is underestimated. Nevertheless, in all these fields (temperature, GPH and precipitation) the main differences between El Niño and La Niña found in the observations are also statistically significant ($p < 0.05$) in the model experiments.

Atmos. Chem. Phys., 6, 4669-4685, 2006

Point-to-point the functional interaction of the inhibition factor with the observed signal and vice versa is significantly raised in the basal dRNA-RIS subunit interaction. This conclusion is consistent with the observed effect of changes of Mg²⁺ concentration and other variables on the extent of GERR12 inhibition. It has been observed, in fact, that all conditions that determine an increased affinity of the ribosomal subunit for dRNA cause a reduction of the inhibitory power of the antibiotic, whereas in the presence of I⁷⁰, whose capacity to increase the mass of formation and dissociation of the 35S subunit complex is well known (Li, 12), seems to enhance the inhibition by GERR12.

In light of the present data, a substantial proportion of GDS from bacterial modification (Fig. 6A), appears C700 (Fig. 6A), A7C, and C764 and somewhat increased sensitivity of A7C, C700, and G602 (Fig. 6A). Some of these bases are the same as those produced by P-site-bound dRNA (19) and by other antibiotics such as streptomycin, kasamycin, and paromomycin, which are traditionally considered P-site inhibitors (Li, 12, 20). For instance, G602 is produced also by paromomycin and streptomycin, whereas A7C, which is affected by aminoglycosides, is produced by kasamycin and streptomycin (Li, 20), and kasamycin and streptomycin also bind to the P-site (Li, 20). The location of the base affected by GERR12 is highlighted within the 3D structure of 16S rRNA (Fig. 6 C and D). Overall, this base does not appear between the platform and the E-site of the 35S subunit. In fact, the finding suggests that inhibition by GERR12 does not involve direct binding to the P-site but probably entails an indirect mechanism of action (see Discussion).

From a synthetic to the fundamental biological process inhibited by the majority of known antibiotics. However, whereas distributed across the ribosome, dRNA binding and decoding in the antibiotic class aminoglycosides and tetracyclines are frequently found to be affected by antibiotics, albeit with different mechanisms, when functionally coupled to protein synthesis, translation, and transcription as early as over 1000 years ago (Li, 24). Thus, the relevance and importance of the present finding in the identification and characterization of the functional properties of GERR12, a unique genetic code for the most selective and efficient inhibitor of prokaryotic 35S initiation complex formation known so far.

The mechanism of translation initiation is unique among the various steps of translation in that it involves the direct binding of dRNA to the ribosomal P-site through a process mediated by initiation factor IF2 (Li, 12). However, within the case of antibiotic factors, which are directly targeted by antibiotics such as kasamycin and streptomycin (Li, 20), kasamycin, paromomycin, and kasamycin (GERR12) (Li, 20, 24), the known antibiotic is capable of forming (directly and) specifically with the IF2-dRNA-RNA interaction. Furthermore, although it is known and well documented in the present study that some of the few antibiotics that are considered "P-site inhibitors" (e.g., streptomycin, and kasamycin) are supported by the present data to be either selective for prokaryotes or specific for a single molecular target, GERR12 was found to target specifically the 35S ribosomal subunit and to interfere indirectly with dRNA binding to the P-site. In fact, the two experiments carried out in this study indicate that GERR12 inhibited both dRNA and overexpressed dRNA binding to the 35S subunit and regardless of whether the coded binding is mediated by the three initiation factors (Fig. 5B). Thus, it can be concluded that the main target of GERR12 inhibition is on the

Deep Indexing: An Innovation in Search and Discovery of Scholarly Material ...



Jim McGinty
Vice-Chairman
Cambridge Information Group

Change in Focus of Indexing

448 T. Ueda, K. Sano, E. Maruyama: Characterization of basin responses in a spatial lattice QDO

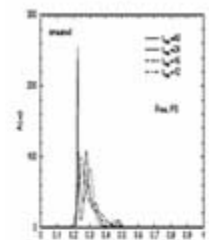


Fig. 2. The result of MEX analysis for the spectral function from the 15 ensemble compared to five grid cells at $N_s = 26$

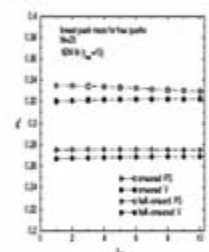


Fig. 3. The result of χ^2 analysis for the spectral function from the 15 ensemble compared to five grid cells at $N_s = 26$

Sub-Article

5 Bratsmanov, et al. The 1989-1991 El Niño cycle in a classical climate model

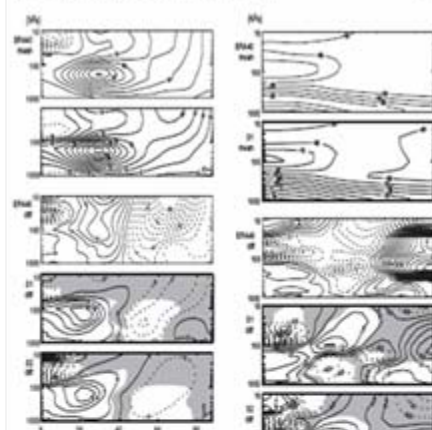


Fig. 4. Sea level and difference between 1987 and 1989 in the North Pacific and North Atlantic. The contours are in cm. The top row shows the sea level and the bottom row shows the difference between 1987 and 1989. The columns represent the North Pacific and North Atlantic. The contours are in cm.

Fig. 5. Sea level and difference between 1987 and 1989 in the North Pacific and North Atlantic. The contours are in cm. The top row shows the sea level and the bottom row shows the difference between 1987 and 1989. The columns represent the North Pacific and North Atlantic. The contours are in cm.

...the sea level and difference between 1987 and 1989 in the North Pacific and North Atlantic. The contours are in cm. The top row shows the sea level and the bottom row shows the difference between 1987 and 1989. The columns represent the North Pacific and North Atlantic. The contours are in cm.

Index Objects

5 Bratsmanov, et al. The 1989-1991 El Niño cycle in a classical climate model

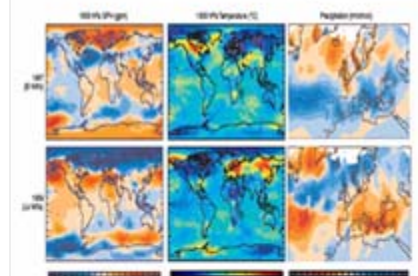


Fig. 6. Observed sea level and difference between 1987 and 1989 in the North Pacific and North Atlantic. The contours are in cm. The top row shows the sea level and the bottom row shows the difference between 1987 and 1989. The columns represent the North Pacific and North Atlantic. The contours are in cm.

March 1987 and 1989. The two waves exhibit the well-known El Niño signature in the North Pacific area such as a strong (weak) Aleutian low for El Niño (La Niña), accompanied by high (low) temperatures in Alaska. Temperature anomalies in northeastern Europe were strongly positive for the El Niño wave and positive for the La Niña wave. The 1989 El Niño field shows a pronounced negative (positive) SLP anomaly in the two waves. This is in contrast to the sea level and temperature effects of El Niño in the North Pacific. The El Niño wave also resembles the strong 1982-83 case (Bratsmanov et al., 2005). A strong precipitation signal is found especially for the La Niña wave, with negative anomalies throughout the Mediterranean area and positive anomalies in northeastern Europe. The El Niño wave shows anomalies of opposite sign, but slightly weaker in magnitude. In general, the south wave is a quasi-symmetric response for the two waves with respect to most of the features, and only partly respects the 1989-1989 wave's 'classical' El Niño cycle signature in the North Pacific and North Atlantic regions.

In order to understand the predicted sea level response in the straits, we analyzed 15-level waves of temperatures at the North Pole (J.F.F. 47°-73°N in SOCOL or 100hPa and 100hPa in the individual ensemble members in the El Niño (Fig. 7). The results for the 1989 El Niño show a strong disturbance (major maximum warming in January). While in 100hPa, temperature dropped again in February and reached very low values in March, the disturbance in 100hPa persisted into spring. In 1989 El Niño, in contrast, the polar temperatures first warmed and then cooled in February, but the last warming time was very pronounced. In the SOCOL experiment, major warming appears in most of the ensembles in both waves, sometimes earlier in one (ensemble in December). The large day-to-day variability across a large wide-scale variability, which hampers the statistical analysis of ensemble means.

Comparisons between simulations and observations for the two individual waves are provided in a next section (and Section 6) and are based on the different observational data. Nevertheless, it is interesting to note that similar to the observations, both models show a response that is close to symmetric, around the respective climatology in the two waves. Model results (especially seas) are compared to the observations in Fig. 2 in the form of the difference between the El Niño wave (1987) and the La Niña wave (1989). The magnitude of the anomalies are generally smaller in the ensemble mean than in the observations.

In addition to the significance of the ensemble mean difference, it is advisable also to look at the distribution function (see also Bratsmanov et al., 2005). Figure 3 shows two-dimensional representations of a grid point over the North Atlantic (30°-50°N, 10°-20°W), which is close to the location of the sea level and sea level difference in the observations.

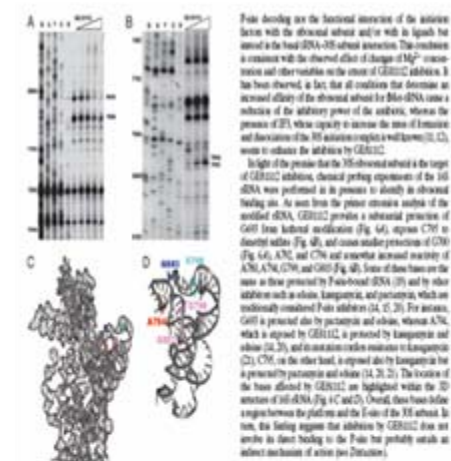


Fig. 7. Observed sea level and difference between 1987 and 1989 in the North Pacific and North Atlantic. The contours are in cm. The top row shows the sea level and the bottom row shows the difference between 1987 and 1989. The columns represent the North Pacific and North Atlantic. The contours are in cm.

Fig. 8. Identification of the 1989/1991 target on the 100-hPa level about the North Atlantic. The contours are in cm. The top row shows the sea level and the bottom row shows the difference between 1987 and 1989. The columns represent the North Pacific and North Atlantic. The contours are in cm.

...the sea level and difference between 1987 and 1989 in the North Pacific and North Atlantic. The contours are in cm. The top row shows the sea level and the bottom row shows the difference between 1987 and 1989. The columns represent the North Pacific and North Atlantic. The contours are in cm.

Create Metadata Linking

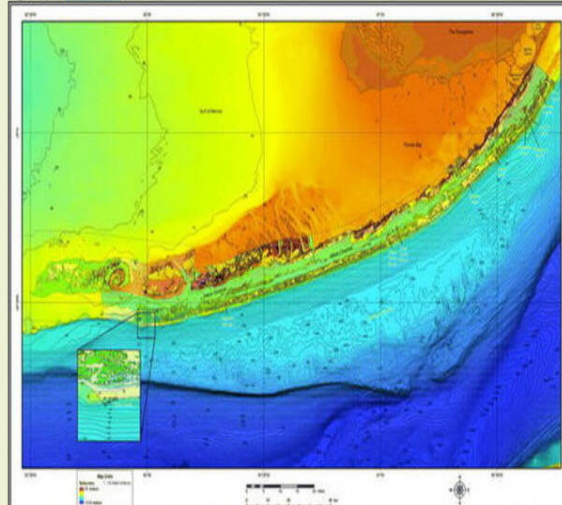
Deep Indexing Provides:

- Image of figure or table
- Category (graph, map, satellite image...)
- Natural language subject terms and statistical descriptor terms, taxonomic, and geographic terms
- Publisher attribution
- Links to rights and permission
- Links to full-text articles

3 of 14 Mark This Record | [Update Marked List](#) | [Save, Print, Email](#)
[View Abstract](#)

Database: CSA Illustrata: Natural Sciences

Image File: [Figure 12. Full Image](#)



Lidz, B. H., Reich, C. D., Peterson, R. L., & Shinn, E. A. (2006). New Maps, New Information: Coral Reefs of the Florida Keys [Figure 12]. *Journal of Coastal Research*, 22, 260-282.
 Publisher: Allen Press, Inc.

Caption Figure 12. Map composite of the USGS habitat and NGDC 10-m-interval bathymetric datasets shows relation between habitats and bathymetric topography. Note location of mid-Hawk Channel patch reefs relative to the two inner-shelf topographic troughs (trough-edge depths 10 and 6 m; the 6-m contour of the northeast trough has been added at upper right). Inset shows offset to the south of outlier reefs from the NGDC topographic high. Offset is an artifact of spatial distortion in deep-water aerial photos. In the printed journal this figure appeared as an insert.

Category [Figure](#); [Map](#); [Bathymetric Map](#)

Title New Maps, New Information: Coral Reefs of the Florida Keys

Author [Lidz, B.H.](#); [Reich, C.D.](#); [Peterson, R.L.](#); [Shinn, E.A.](#)

Source *Journal of Coastal Research*, Vol. 22, No. 2, pp. 260-282. Mar 2006.

Descriptors **Object Subject Terms:** Geographic location Inner-shelf topographic troughs Patch reefs Trough-edge depths (m)

New Search Using Marked Terms: Use AND to narrow Use OR to broaden

Publisher Allen Press, Inc., 810 East Tenth St., PO Box 1897, Lawrence KS 66044

Why Index Figures/Tables

- Figures and tables represent the distilled essence of research—the closest thing to raw datasets
- Researchers want access to this data
- This information is invisible/not addressable

Researcher Response ...

Overwhelmingly, respondents said the ability to search for specific types of objects would make a difference in their search and discovery processes...

--save time

--work more efficiently

--aid in presentations

--find more relevant results."

Tenopir, C., & Sandusky, R.J. (2006). The Value of CSA Deep Indexing for Researchers - Draft Final Report

Information service within CSA Illumina which provides:

- Web-based access to indexed tables/figures
- Searching by type of table/figure
- Searching/linking to enhanced abstracts
- Linking from table figures to full-text articles
- Linking to rights/permissions



**Enhanced search and discovery
via increasing precision and relevancy**

What's Causing Enhanced Precision/Relevancy

- Enhanced Citations
- Enhanced Abstracts
- Object Records
- New Search Path

Citation Display with “pinkies”

All Publication Types 46136

Journals [29283](#)

Peer-Reviewed Journals [18938](#)

Conferences [5460](#)

Books [2721](#)

[More >](#)

[Mark](#) or [Clear](#) all on page | [Update Marked List](#) | [Save, Print, Email](#) | **RefWorks**

Sort by: Most Recent First

◀ Previous 1 [2](#) [3](#) [4](#) [5](#) Next ▶

Record #

1. [Invertebrate Colonization Patterns in a Mediterranean Chilean Stream](#)

[Figueroa, Ricardo](#); [Ruiz, Victor](#); [Niell, Xavier](#); [Araya, Elizabeth](#); [Palma, Alejandro](#)

Hydrobiologia [Hydrobiologia]. Vol. 571, no. 1, pp. 409-417. Nov 2006.

The macrozoobenthos colonization process on artificial substrata in lotic environments was evaluated. Two seasonal periods, autumn-winter and spring-summer, of a relatively undisturbed fluvial system, the Estero Nonguen (VIII Region, Chile), have ...



[View Record](#) | [Full-Text Linking](#)

Database:

CSA Illustrata: Natural Sciences

Object Descriptors:

[Altitude \(m\)](#) | [Autumn-winter](#) | [Colonization](#) | [Distance from source \(m\)](#) | [General characteristics of sampling stations](#) | [Lineal colonization](#) | [More...](#)

2. [Effects of flow on meiofauna colonization in artificial streams and reference sites within the Illinois River, Arkansas](#)

[Smith, Freese](#); [Brown, Arthur V](#)

Hydrobiologia [Hydrobiologia]. Vol. 571, no. 1, pp. 169-180. Nov 2006.

... of drifting meiofauna (potential colonists of the *benthos*) were low (5 no. I super(-1)) and similar among artificial channels and reference sites regardless of flow rates ($F_{sub(1,18)} = 2.19, p = 0.1407$). Although densities were low, the ...



[View Record](#) | [Full-Text Linking](#)

Database:

CSA Illustrata: Natural Sciences

Object Descriptors:

[Abundant benthic taxa](#) | [Benthic dipterans](#) | [Benthic meiofauna](#) | [Benthos](#) | [Colonization period \(d\)](#) | [Densities \(no./L\)](#) | [More...](#)

1 of 1 Mark This Record | [Update Marked List](#) | [Save Print Email PdfWorks](#)
[View Abstract](#) | [Table of Contents](#) | [Full-Text HTML](#) | [Openly Full-Text](#) | [SFX](#)

Links to Full-Text

Database CSA Illustrata: Natural Sciences

Title Conservation and Development in Amazonian Extractive Reserves: The Case of Alto Jurua

Author [Ruiz-Perez, M](#); [Almeida, M](#); [Dewi, S](#); [Lozano Costa, EM](#); [Pantoja, MC](#); [Puntodewo, A](#); [Arruda Postigo, Ad](#); [Andrade, AGd](#)

Source Ambio [Ambio]. Vol. 34, no. 3, pp. 218-223. May 2005.

Objects



Figure 1.

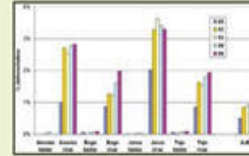


Figure 2.

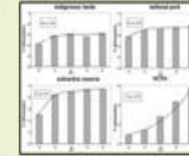


Figure 3.

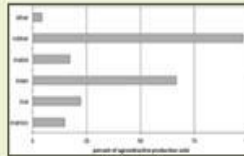


Figure 4.

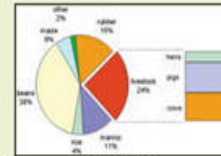


Figure 5.

Year	Number	Area (km ²)	Population
1990	4	21 630	13 912
1992	9	22 008	17 862
1997	11	25 108	21 562
1998	12	31 584	25 562
1999	13	32 104	25 962
2000	16	34 079	28 992

Source: CNPT-IBAMA and Igesias (18).

Table 1.

Abstract Extractive reserves constitute an innovative approach to match conservation and development objectives, which were originally envisaged as part of a land struggle by forest dwellers in Brazil. In spite of the idea's popularity and the attempts to apply the concept to different tropical regions, there has been little analysis of the combined conservation and development performance of extractive reserve programs. We present a detailed analysis of deforestation and demographic and socioeconomic changes in Alto Jurua, the first extractive reserve created in Brazil in 1990. Forest cover has remained fairly stable. Population has declined slightly, with some internal displacements. The cash economy base has shifted from the original rubber production to a diversified portfolio of agriculture and livestock, and there has been a dramatic rise in nonagrarian income. We conclude that the Reserve represents a very dynamic setting with positive conservation and development outcomes during its first decade.

Descriptors **Article Subject Terms:** Conservation Forests Deforestation Demography Development Rubber Socio-economic aspects Livestock Tropical forests Population dynamics Income

Article Geographic Terms: Brazil Brazil, Amazonia

Object Descriptors **Object Subject Terms:** Area (km²) Average cows per family Demographic changes Extractive reserves Livestock income expanded Number of cows (no.) Percentage changes in livestock (%) Percentage deforestation (%) Percentage of total agro-extractive production sold (%) Percentage rural (%) Primary sector Rural population index Structure of cash income Time (yr)

Object Geographic Terms: Brazil

New Search Using Marked Terms: Use AND to narrow Use OR to broaden

Publisher Royal Swedish Academy of Sciences

Classification D 04705 Conservation; M3 1120 Land; EE 10 General Environmental Engineering

Object Thumbnails



Article Descriptors



Object Descriptors



Record View Return to View Record

Abstract Mark This Record | [Update Marked List](#) | [Save](#) | [Print](#) | [Email](#) | [PDFWorks](#) | [View Abstract](#) | [Table of Contents](#) | [Full-Text HTML](#) | [Openly Full-Text](#) | [SFX](#)

Discovery Links

Database CSA Illustrata: Natural Sciences Index

Image File [Figure 5. Full Image](#)

Category	Percentage
beans	38%
livestock	24%
manioc	11%
rubber	15%
maize	6%
rice	4%
other	2%

Ruiz-Perez, M., Almeida, M., Dewi, S., Lozano Costa, E. M., Pantoja, M. C., Puntodewo, A., et al. (2005). Conservation and Development in Amazonian Extractive Reserves: The Case of Alto Jurua [Figure 5]. *Ambio*, 34, 218-223. Publisher: Royal Swedish Academy of Sciences

[Get Permissions](#) Copyright Clearance Center

Caption Figure 5. Structure of cash income from primary sector-based activities, with livestock income expanded in the bar

Category [Figure](#); [Graph](#); [Pie Chart](#)

Title **Conservation and Development in Amazonian Extractive Reserves: The Case of Alto Jurua**

Author [Ruiz-Perez, M.](#); [Almeida, M.](#); [Dewi, S.](#); [Lozano Costa, E.M.](#); [Pantoja, M.C.](#); [Puntodewo, A.](#); [Arruda Postigo, A.d.](#); [Andrade, A.G.d.](#)

Source *Ambio*, Vol. 34, No. 3, pp. 218-223. May 2005.

Object Descriptors Object Subject Terms: Cash Income Beans Rice Maize Corn Rubber Manioc Livestock Hens Pigs Cows

New Search Using Marked Terms: Use AND to narrow Use OR to broaden

Publisher Royal Swedish Academy of Sciences, P.O. Box 50005, Stockholm S-104 05

Links to Full Text

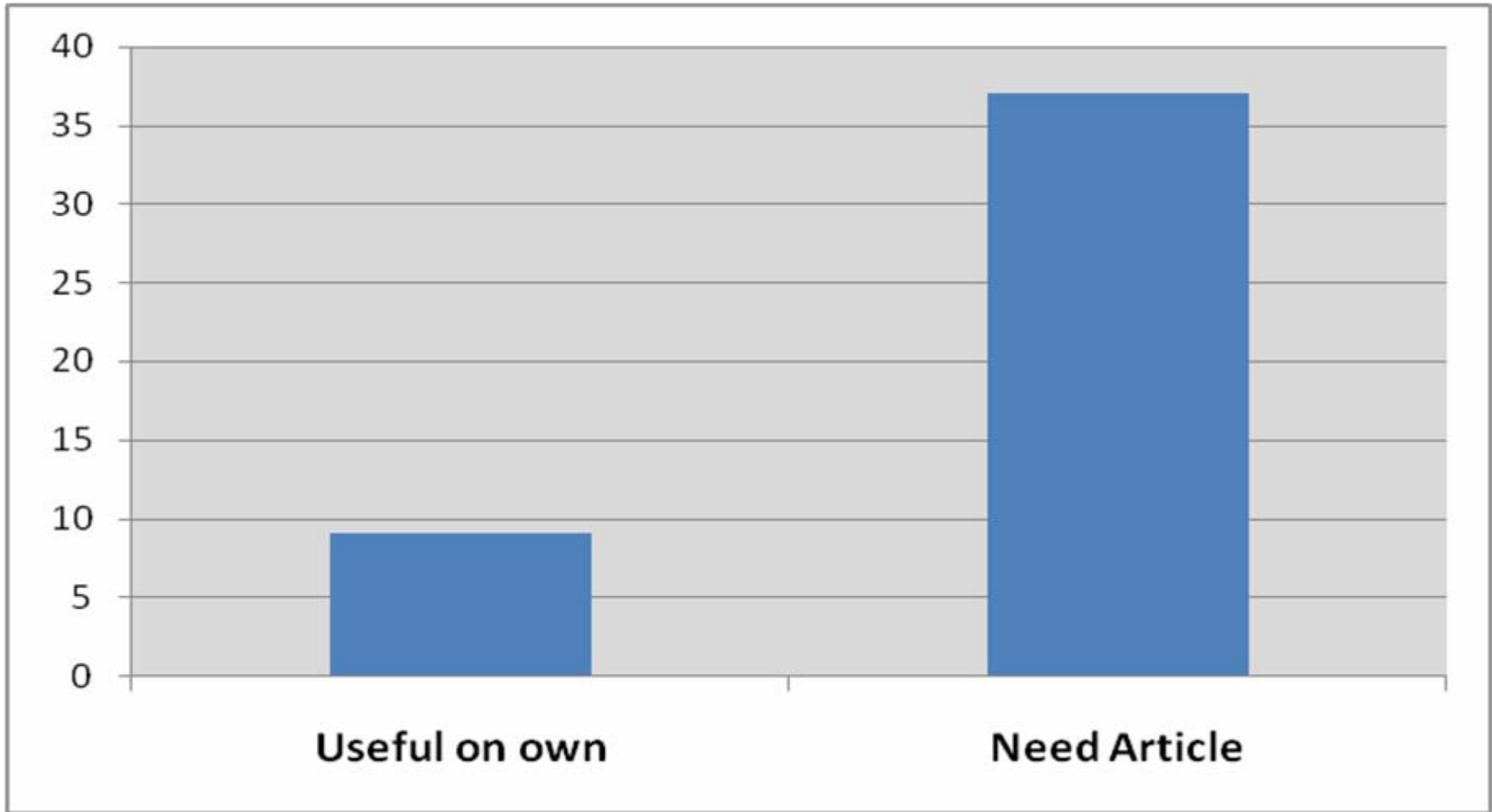
Attribution

Rights Management

Category

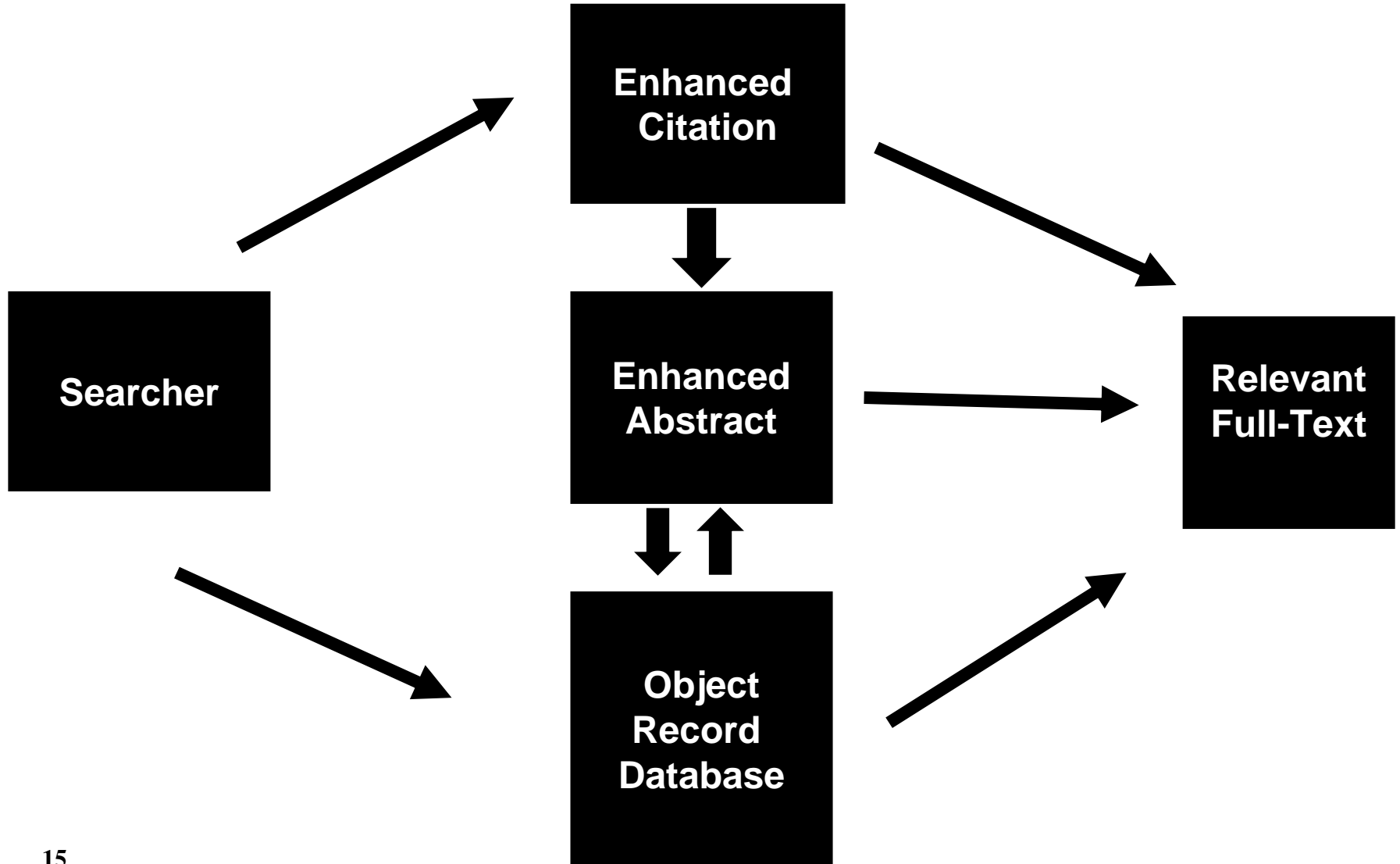
Object Descriptors

Usefulness of Objects with and without Corresponding Articles



Tenopir, C., & Sandusky, R.J. (2006). *The Value of CSA Deep Indexing for Researchers*,
14 figure 59 - Draft Final Report

Enhancing Precision in Full-Text Access



What Customers/Users Are Saying

- “It provides another way to evaluate and winnow out data without overwhelming users and having to take extra steps to get it—and for visual/graphic data in the applied sciences that is really important.”
— *Lisa Dunn, Head of Reference*
Arthur Lakes Library, Colorado School of Mines
- “I waste a lot of time looking through papers which look like they contain some data, but they don’t. I definitely see this database as a significant improvement”
— *Dr. Maria Prokopenko*
Princeton University

What Customers/Users are Saying

- “Not only could you find this information... but link ... back to the article (it) came from ... This is definitely going to make our jobs much easier.”
— *Van Afes, Director*
Waldmann Memorial Library, New York University.
- “It’s much easier to find the information; it’s much, much better.”
— *Dr. Marco Colombini*
University of Maryland
- “I believe that CSA Illustrata represents a major innovation access to scholarly information and have been actively encouraging students and staff at the University of Queensland to utilize this unique resource.”
— *Keith Webster*
University of Queensland Library

What Will Deep Indexing Mean for Secondary Publishing

- Discovery/illumination of article/journal
- Greater precision/relevancy provided to users
- Enhanced probability of citing ... article/author/journal
- Additional service to authors
- Possibility of modular offerings



**Increase usage/satisfaction
of full-text offerings**

What will Deep Indexing Mean to Librarians

- Additional Capability for Faculty/Researchers
 - Precision/Relevancy*
 - Time Savings*
- Enhanced ROI from Full-Text Purchases
- Journals Selection Factor

Contact ProQuest

Mark Hyer

Vice President of Secondary Publishing

(240) 752-7126

mark.hyer@proquest.com

Next Step: View Video

“The Power of Deep Indexing”

www.proquest.com/go/illustrata